Wavefront sensors for control and process monitoring in optics manufacture.

D. R. Neal[†], D. J. Armstrong, and W. T. Turner

WaveFront Sciences, Inc., 15100 Central S.E., Albuquerque, NM 87123
Phn: (505)275-4747 FAX: (505)275-4749 email: drneal@wavefrontsciences.com

Abstract

Measurement is an integral part of optics manufacture, where grinding and polishing steps are linked iteratively with the testing steps. While numerous test methods have been developed, many of these are prone to vibration effects that limit their application to in-situ monitoring, or have other limitations. We have applied Shack-Hartmann wavefront sensors to the problems of optics measurement. We have developed an instrument that allows testing in common configurations, and also provides new ways to test optics. The current device is extremely sensitive. We have demonstrated this device for testing various optical elements including lenses, mirrors and laser rods.

Keywords: Wavefront sensor, Shack-Hartmann sensor, micro-optics, diffractive optics, interferometers, beam profiler, beam quality, optics testing

1. Introduction

Fabrication of optical elements usually involves iterative steps of grinding and polishing, interspersed with measurement of the surface or optical figure, and then repeated polishing. Tests during fabrication, and for final quality inspection and grading, are integral to the manufacture of optical components, and require simple and inexpensive measurement methods. Numerous methods have been developed over many years to carry out these measurements[1].

One key requirement for these diagnostics is the ability to measure the wavefront imposed by the optic under test. This usually requires some form of interference phenomenon, although other tests can also be used. Some of these tests, such as knife edge and other schlieren techniques are simple, highly sensitive, and provide qualitative information sufficient for in-process monitoring[1]. For quantitative measurements of surfaces or transmitted wavefronts, an interferometer is most commonly used. Interferometers are thoroughly developed, and generally include automated analysis software to make data acquisition and analysis a straightforward process[2]. In order to provide a measurement of the surface shape at a large number of points, most interferometers use a phase-shifting algorithm, where the reference mirror is moved by a small amount and several successive measurements are taken. This eliminates the need for fringe interpretation and provides quantitative results[3].

Although interferometers are a standard measurement tool in the optics industry, the added complexity of phase shifting, as well as the high quality required of all intermediate optics, make these devices large and expensive. Furthermore, they must be used in vibration free environments so that there is no change in the optical phase during the 1–2 second measurement period. Therefore, they cannot readily be used on the shop floor during fabrication, and are relegated to statistical sampling or laboratory use.

For optics fabrication, a wavefront sensor might provide a simple, inexpensive, measurement method, yet yield quantitative results with resolution equal to that of interferometers. One example is the Shack-Hartmann sensor[4,5], a wavefront sensor based on an array of microlenses that dissects an incoming wavefront into a number of segments. Each "lenslet" creates a focal spot on a detector array. Because light travels in a straight path normal to the wavefront, the position of these focal spots is related to the average wavefront slope over each lenslet aperture. Thus the pattern of spots at the focal plane contains information about the spatially-resolved wavefront slope that can be integrated to reconstruct the wavefront. Because all of the information can be collected rapidly in a single frame, the sensor is very insensitive to vibration. It is also smaller and lighter than an interferometer, and has a wider variety of applications.

We have applied this wavefront sensor technology to measuring various optical elements by building an integrated system that is easily configured for a wide

---

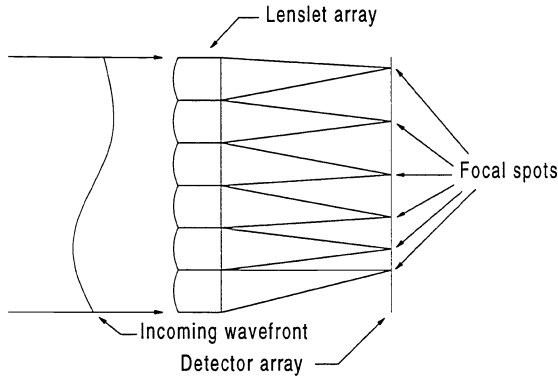[†] Formerly at Sandia National Laboratories, Albuquerque, NM

Figure 1 - Basic configuration of a wavefront sensor.

variety of test situations. Flat, spherical, cylindrical, aspheric, and anamorphic optics, as well as optics with arbitrary shapes, can all be easily tested with a few simple configurations of this instrument. In addition, the same instrument can be used to characterize laser beams by measuring the spatial intensity[6] profile and the phase, and it can accept beams with diameters ranging from 1–100 mm.

The body of this paper will present the design of an instrument for testing large diameter optics using a wavefront sensor, and discuss several applications and test examples.

2. Wavefront sensor fundamentals

A wavefront is defined as the surface that is normal to the direction of propagation of light, and represents all points of the oscillating electric field having equal phase. At an arbitrary point in time, the electric field of a coherent light wave propagating along the z-axis can be described by a time-independent complex amplitude

$$\widetilde{E}(x,y,z) = \left|\widetilde{E}(x,y,z)\right| e^{\frac{j2\pi\varphi(x,y,z)}{\lambda}}, \qquad (1)$$

where the phase φ is measured with respect to a reference point on the z-axis. Because of rapid temporal oscillations at optical frequencies, it is not possible to directly measure the electric field. However, by using a Shack-Hartmann wavefront sensor, one can indirectly reconstruct a discrete approximation to the electric field at a given plane normal to the z-axis.

The Shack-Hartmann sensor shown in Firgure1 provides a method for measuring the phase and intensity of an incident light wave. The sensor consists of a lenslet array and detector, usually a CCD camera, with the lenslet array placed one focal length from the detector. Each lenslet defines a subaperture, and focuses light from a small portion of the incident wavefront onto a different position on the detector. By locating the
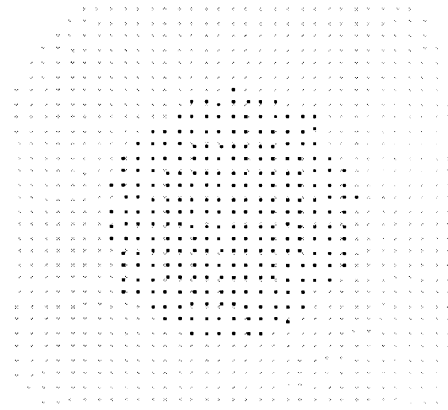

Figure 3 Data from Shack-Hartmann sensor showing calculated centroid positions. The light gray spots are the centroid positions of the calibration beam.
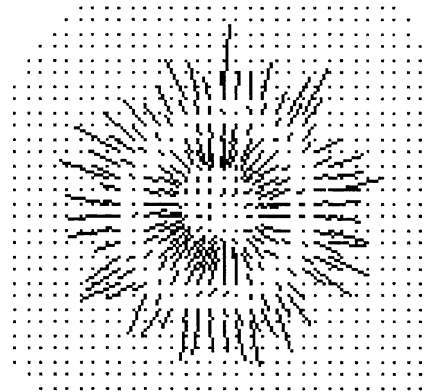

Figure 2 - Vector plot showing wavefront slopes for an optic under test. The vector represents the magnitude and direction of the wavefront slope over each measurement point. The RMS wavefront slope was 0337 mr in the x-direction and 0.38 mr in the y-direction.

position of each of these focal spots, the average wavefront slope over the lenslet is accurately determined, with no measurement errors introduced by aliasing. (Recall the mean value theorem.) The wavefront itself must be reconstructed by integrating these wavefront slope measurements.

Measuring wavefronts with a Shack-Hartmann sensor requires several steps of data reduction. First, the sensor must be calibrated by placing it in a suitable reference beam, acquiring and digitizing the data. The resulting reference image, consisting of focal spots at the plane of the detector, must be divided among a set of small windows. Each window contains many detector pixels, and is centered on the peak of a focal spot, with one
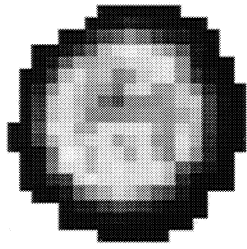
Figure 4 - Intensity map for test optic. The intensity is uniform over most of the aperture.

window per lenslet. Once the windows have been found, a centroid is computed using a center-of-mass algorithm

$$\hat{\rho}_{x,l} = \frac{\sum\limits_{(i,j)\in W_l} I_{ij} x_{ij}}{\sum\limits_{(i,j)\in W_l} I_{ij}},$$

(2)

where the indices i,j refer to pixels, and $I_{i,j}$ is the intensity in the pixel located at $x_{i,j}$. A sum is made over the pixels in each window W_l, where l indicates a particular lenslet of the intensity-weighted locations. (When not mentioned explicitly, similar equations hold for the y-axis.) This results in a calibration set of centroids, $\hat{\rho}_{x,l}\big|_{CAL}$ and $\hat{\rho}_{y,l}\big|_{CAL}$. The sensor is now completely calibrated and is ready for acquisition and measurement of actual data. Note that the calibration beam need not be collimated, as long as its characteristics are well known; results are then deviations from this reference.

The first step in analyzing real data is the same as that for the calibration data. A data set is acquired and digitized and then centroids are computed using the windows calculated in the calibration step. A typical image is shown in Figure 3. Once these centroids are obtained, and the lenslet to detector distance L is known, the wavefront slopes can be calculated,

$$\theta_{x,l} = \frac{\partial \varphi}{\partial x} = \frac{\hat{\rho}_{x,l} - \hat{\rho}_{x,l}\big|_{CAL}}{L}.$$
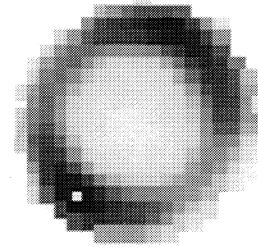
(3)

An example of these data are shown in Figure 2.

Figure 5 - Phase map for test optic. In this case spherical aberration dominates the phase structure. The RMS wavefront error was 0.208 μm, and the peak-to-valley wavefront error was 0.86 μm.

The final step is reconstruction of the wavefront ϕ. This is accomplished by solving of the gradient equation

$$\nabla \varphi = \frac{\partial \varphi}{\partial x} \hat{i} + \frac{\partial \varphi}{\partial y} \hat{j},$$

(4)

where the data provide values for the wavefront gradient,

$$\frac{\partial \varphi}{\partial x}\bigg|_l = \theta_{x,l} \quad \text{and} \quad \frac{\partial \varphi}{\partial y}\bigg|_l = \theta_{y,l}.$$

(5)

Here θ_x and θ_y are the measured slope data at lenslet l. The reconstruction proceeds by finding a set of φ_l values that obey the above equations. Commonly used methods include least-squares procedures and marching methods[7].

One method that has the advantage of accounting for the intensity distribution as well as the phase slopes is known as the modal reconstructor method. In this method the data are fit to the derivatives of an analytical surface described by an expansion in terms of a set of basis functions. One simple case is the use of a polynomial expansion. Thus the phase φ might be described by a series of polynomials such as

$$\tilde{\varphi}(\tilde{x}, \tilde{y}) = a_{00} + a_{10} Z_{10}(\tilde{x}, \tilde{y}) + a_{11} Z_{11}(\tilde{x}, \tilde{y}) +$$
$$+ a_{20} Z_{20}(\tilde{x}, \tilde{y}) + a_{21} Z_{21}(\tilde{x}, \tilde{y}) +$$
$$+ a_{22} Z_{22}(\tilde{x}, \tilde{y}) + \cdots + a_{nk} Z_{nk}(\tilde{x}, \tilde{y}) + \cdots,$$
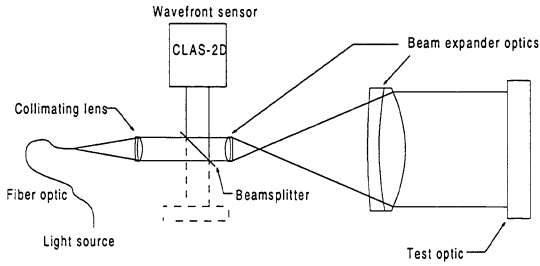
(6)

Figure 7 - Layout of optical metrology system. The fiber-coupled source is a laser or halogen lamp. In this "active" configuration using an internal source, optics can be tested by placing them adjacent to the beamsplitter, or after the beam expander.

where the polynomial $Z_{nk}(\tilde{x}, \tilde{y})$ is the kth Zernike polynomial of nth order. Because Zernike polynomials are only defined over a unit circle[8], the tilde denotes normalization by a scale factor, usually the half-width of the detector array. Zernike polynomials are a convenient basis set, but other polynomials such as Hermite, or even non-orthogonal polynomials, can be used as well. Once the phase is described in this manner, the derivatives of the phase are easily determined by

$$\frac{\partial \varphi}{\partial x} = a_{10} \frac{\partial Z_{10}}{\partial x} + a_{11} \frac{\partial Z_{11}}{\partial x} + \cdots + a_{nk} \frac{\partial Z_{nk}}{\partial x} + \cdots,$$

(7)

with a similar expression for the y-derivative. Equation (7) is then fit to the wavefront slope data using a least-squares method. Since Eqn. (6) determines the wavefront phase in terms of these a_{ij} (with an arbitrary constant of integration, a_{00}), the complete wavefront has been determined. Figure 4 and 5 illustrate typical intensity and phase distributions obtained by the method outlined here.

3. Measurement instrument design

To use a wavefront sensor to measure optics, a few more components are necessary. First, the size of the optic to be tested may be incompatible with the dimensions of the wavefront sensor, so a beam expander may be needed to reformat the image size. In addition, some type of source is required to provide well characterized light for the test. To address these requirements, we have developed a simple, modular instrument that contains all elements needed for optics testing.

3.1 Optical design

There are several requirements which must be met in the design of an optical test instrument. Since most optics and optical systems are completely passive, the sensor must provide an internal light source. Optics vary widely in size, so the system must operate over a large range of diameters. Furthermore, overall instrument size is important, so that minimum space is needed for setting up the instrument.

The system we developed, consistent with these principles, is shown in Figure 7. This system includes a beam expander to increase the beam diameter to 100 mm, an integral light source, and a CLAS-2D[9] wavefront sensor. The light source is a fiber -optic-coupled lamp or laser that is collimated with an achromatic lens. This light is directed through the beam expander to the optic under test (single pass for reflective optics, double pass for transmissive). The light returned from the test optic passes through the beam expander in reverse, and is directed by a
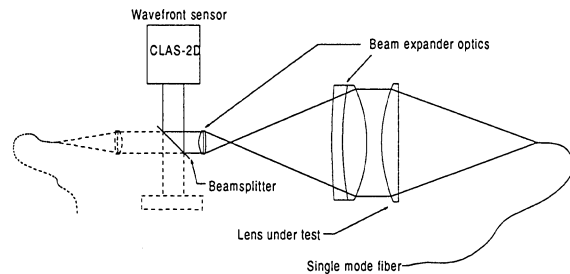

Figure 6 - A focusing optic can be tested using a single mode fiber as a point source. In this "passive" configuration, there are no reference optics and no internal light source.

beamsplitter onto the wavefront sensor. This allows measurements to be made using a common optical path. In this "active mode," the system is calibrated by placing a single (presumably flat) mirror of known quality at the test location, and recording a reference wavefront. This wavefront serves as the calibration wavefront for all subsequent tests. Because this reference wave contains aberrations from the beam expander and other optics, these aberrations are removed from all subsequent measurements.

For testing extremely high quality optics, it may be desirable to avoid the use of any reference optics. However, since the beamsplitter and beam expander optics are not of exceptionally high quality, some reference beam is needed. This can be created using a single mode fiber or a pinhole to provide an effective point source of light. As long as the fiber is truly single mode, or the pinhole is the limiting aperture, the

Quantity	Unit	Case 1	Case 2	Case 3	Case 4	Case 5
Magnification		1	0.05	0.1	0.05	0.1
Lenslet focal length	mm	8.1896	8.1896	8.1896	2	2
Lenslet size	mm	0.144	0.144	0.144	0.072	0.072
Lenslet f#		56.9	56.9	56.9	27.8	27.8
Number of lenslets X		45	45	45	89	89
Number of lenslets Y		34	34	34	66	66
Pixel size	um	9.8	9.8	9.8	9.8	9.8
Sensitivity	mr	0.0120	0.0006	0.0012	0.0025	0.0049
wavefront	um	0.0116	0.0006	0.0012	0.0017	0.0033
Waves at 0.633 nm		0.0183	0.0009	0.0018	0.0026	0.0053
Dynamic range	mr	8.79	0.44	0.88	0.90	1.80
wavefront	um	57.0	2.8	5.7	5.8	11.5
Waves at 0.633 nm		90.0	4.5	9.0	9.1	18.2

Table 1- Optical metrology system parameters.

wavefront leaving this source is a true spherical wave with known curvature. In this "passive mode", the external source can serve as an absolute reference beam. To use this with the optical metrology system, the beam expander is adjusted using a micrometer positioning mount for the second (large) lens so that it focuses at a point in space some distance from the instrument. Typically this may be 5-20 m away. The single mode fiber or pinhole is placed at this location and a reference beam recorded. The beam expander is then adjusted back to the collimated lens position for optics testing. Thus an absolute reference wavefront has been recorded that has no aberrations from extraneous optics, and calibrates for optical errors in the instrument itself.

This metrology system is quite versatile. Both small and large optics can be tested, and the system can be used for either optics or laser testing. For example, in testing a positive lens there are two useful configurations, and the system has all of optical elements needed for both. In the active configuration shown in Figure 7, the lens is tested in double pass, with the light returned from a convex reference sphere. This test assumes that the quality of the sphere is known. We typically use ball bearings, and have found that they are nearly perfect spheres and have excellent surface quality. The other configuration is depicted in Figure 6. In this passive case the, end of the optical fiber is placed at the focal point of the lens.

It is also straightforward to test laser beams or any other optical system where the system under test provides the light. In this case the internal source is simply turned off. Note that the arrangement of the instrument is such that it allows direct access to the wavefront sensor through the beamsplitter. Small optics or small diameter laser beams may be tested as well. With the source turned on, the beamsplitter will provide light that can be used for testing from both the small and the large apertures.

This type of beam expander has conjugate image planes one focal distance away from each of the lenses. In order to achieve good imaging, the mirror (or optic)

under test must be placed at the appropriate object plane. This plane can be moved closer to the input lens, with a corresponding move of the image plane, within some limits. For our initial instrument, mechanical considerations prevented placing the sensor at this plane. However, for most optics, the system uses essentially collimated beams, so positioning exactly at an image plane is not important.

Three important parameters in this design are the sensitivity and dynamic range of the sensor, and the magnification of the beam expander. It will be shown below that the magnification affects both the sensitivity and dynamic range, and thus drives the design of the instrument.

Sensitivity (or resolution) is related to the minimum measurable shift of the focal spot position in the image plane of the wavefront sensor. The focal spot for each lenslet is fairly large, covering several pixels. This provides the centroid algorithm of Eqn. (2) with a fairly large sample base, typically 50-100 pixels. Thus pixel noise effects are reduced through averaging, and a very accurate measure of the centroid can be deduced. Sensor noise and lenslet-to-lenslet optical cross-talk usually limit centroiding accuracy to about 1/100 of a pixel element[10,11]. From Eqn. (3) the minimum measurable wavefront slope, θ_{min}, can be calculated as $\theta_{min}=p/(100f)$, where p is the pixel size and f the lenslet focal length. This is often referred to as the sensitivity or resolution of the instrument, since it represents the minimum resolvable measurement that can be made. For a Shack-Hartmann sensor, it is also the same as the precision or repeatability, since successive measurements will yield different noise realizations whose average is still limited to about 1/100 pixel. The absolute accuracy of the sensor is related to the ability to create an accurate reference beam. This relies on an external reference source. There are several methods for creating very good reference sources, including high quality beam expanders, pinhole diffraction and single mode fibers. These are routinely employed in calibration of the sensor to better than 1/100 of a wave.

Across any given lenslet, the wavefront error introduced by this noise level is just $\theta_{min}d$, where d is the lenslet diameter. For a typical wavefront sensor, as shown in the first column of Table 1, this comes to 1.7 nm wavefront error across a single lenslet, or better than $\lambda/350$ for $\lambda = 633$ nm. It is not possible to realize this resolution across the whole aperture, however, since the wavefront must be reconstructed by connecting a large number of measurements that each have this measurement error. For most wavefront reconstructors, attempting to solve Eqn. (4) involves a random walk addition of the errors. For a large number of samples,

N, across the aperture this implies Gaussian statistics. Hence the overall wavefront error across the aperture is given by

$$\varphi_{min} = \theta_{min} d \sqrt{N}$$

(8)

For the wavefront sensor listed in Table 1, this gives 0.018 μm of wavefront error across the aperture (using d=0.144 mm and N=45) or about 1/50 wave at 633 nm. This agrees well with experimental repeatability derived from examining successive measurements.

The largest wavefront slope the sensor can measure, or dynamic range, is limited in several ways. Clearly, when adjacent focal spots collide, no meaningful measurement can be made. However, the centroid algorithm works only over a small region of interest that is usually defined when the reference image is stored. If the focal spot wanders outside this region of interest, then inaccurate centroid values will result. There are ways to extend this range by tracking the location of the region of interest, but this is usually too complicated for normal operation. The size of these regions of interest is (for a collimated reference beam) just the distance between the focal spots d. Thus the dynamic range is simply $\theta_{max} = d / 2f$. For the wavefront sensor described in the first column of Table 1, this is 8.79 mr total wavefront slope, or 1.26 μm per lenslet. Across the whole aperture, the maximum wavefront error is

$$\varphi_{max} = \theta_{max} Nd,$$

(9)

which gives 57 μm for the sensor in Table 1. This is over 90 waves at 633 nm! The ratio of dynamic range to minimum resolution is ~5000. It is this large ratio that often makes this instrument interesting compared to an interferometer. It means that if the appropriate lenslet design can be used, then an instrument with both high sensitivity and large dynamic range can be built.

The magnification of the optical system, however, plays a key role in determining these parameters. It determines the size of the optics that can be tested, and it directly affects the dynamic range and sensitivity.

To understand the effects of magnification, we can examine the ray matrix for the beam expander shown in Figure 7. When propagating from object plane to image plane, this matrix can be written,

$$\begin{bmatrix} r_o \\ \theta_o \end{bmatrix} = \begin{bmatrix} M & 0 \\ 0 & 1/M \end{bmatrix} \begin{bmatrix} r_i \\ \theta_i \end{bmatrix},$$

(10)

where M is the magnification, and r_i, θ_i are the displacement and angle of the input ray as measured from the optical axis. This tells us that rays entering the optical system at angle θ_i experience angular magnification and exit at angle $\theta_o = \theta_i/M$. It is θ_o that is directly measured by the wavefront sensor. Therefore, the measured input angle is given by $\theta_i = M\delta/f$, where δ is the shift of the focal spot at the detector plane, and f is the focal length of the lenslet array. Across a lenslet, this leads to a slope sensitivity given by

$$\theta_{min} = \frac{Mp}{100f}.$$

(11)

Across the entire aperture for a sensor with N elements this gives

$$\varphi_{min} = \frac{pdM\sqrt{N}}{100f}.$$

(12)

The dynamic range is similarly affected, thus

$$\theta_{max} = \frac{Md}{2f},$$

(13)

and the maximum wavefront error is

$$\varphi_{max} = \frac{NMd^2}{2f}.$$

(14)

This has a number of implications. For testing large optics, the magnification is usually a small number, since the light must be reduced from the size of a large lens down onto the detector. Typically this is 0.05 to 0.1 and the angular magnification is 10 to 20. This greatly enhances the sensitivity of the system. However, it also reduces the dynamic range by the same factor.

The optical system design consists of selecting a set of parameters that produces the desired dynamic range and sensitivity. An example spreadsheet showing these calculations is presented in Table 1.

When designing the sensor, magnification is constrained by dimensions of the detector, and the diameter of the optic to be tested. In Table 1, the first case is for a 8.1896 mm focal length wavefront sensor with unity magnification. The next two cases are for a 8.1896 mm lenslet array (the standard CLAS-2D) using a Costar CVM-50 camera with a 6.45 x 4.8 mm focal plane. To view the entire optic with this camera, the object height
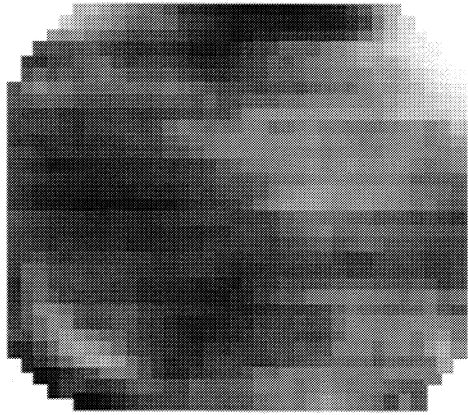
Figure 9 - Phase map for flat optic calibrated against itself. The phase structure is due to thermal variations in the room. The RMS wavefront error is 0.009 μm, and the P-V WFE is 0.095 μm.

Figure 10 - Homogeneity test for a fused silica rod. RMS wavefront error was .0142 μm and the P-V WFE was 0.1774 μm.

is chosen as 100 mm, with the image plane size to match the smallest camera dimension. Two cases are shown in the table to account for use with a different camera with a larger focal plane array. For the CVM-50 camera, a magnification of .05 is needed. For each of these two cases, the parameters are calculated for two different lenslet arrays with focal lengths of 2 mm and 8.2 mm.

In Table 1 the effect of the magnification is clearly evident. The basic wavefront sensor has a large dynamic range of 90 waves at 633 nm, while maintaining sensitivity of better than $\lambda/50$. However, with magnification of 0.05, the dynamic range drops to 4.5 waves at 633 nm, and sensitivity increases to better than $\lambda/1000$. The dynamic range is increased somewhat by using a 2 mm focal length lenslet array, giving 9 and 18 waves respectively for magnifications of 0.05 and 0.1, while still maintaining a very sensitive system. Clearly the dynamic range limits the design of this system.

Because the 8.1896 mm focal length lenslet array was intended for measuring wavefronts of laser beams, it is not optimized for optical characterization. Fortunately, designing these arrays is a straightforward process using binary optics or other approaches. A lenslet array with smaller f/# would increase the dynamic range considerably, while sacrificing some sensitivity. Nonetheless, when used with small magnification, sensitivity is not always important. Besides changing lenslet design, there are a number of other techniques that can be used to increase the dynamic range that can be implemented in the software data analysis.
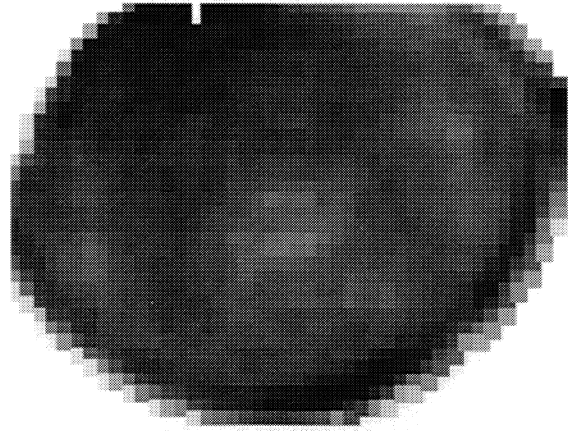
3.2 Performance

Figure 9 is the phase map for a four inch diameter, certified $\lambda/100$ flat mirror we use as a reference flat for optics testing, where the sensor was calibrated using this same mirror. Testing the optic against itself provides a measure of the sensitivity, or noise level, of the wavefront sensor. In this measurement the phase structure was dominated by air turbulence due the presence of nearby heater vents. We have seen an order of magnitude smaller phase structure when the heater was off and the room temperature was allowed to stabilize.

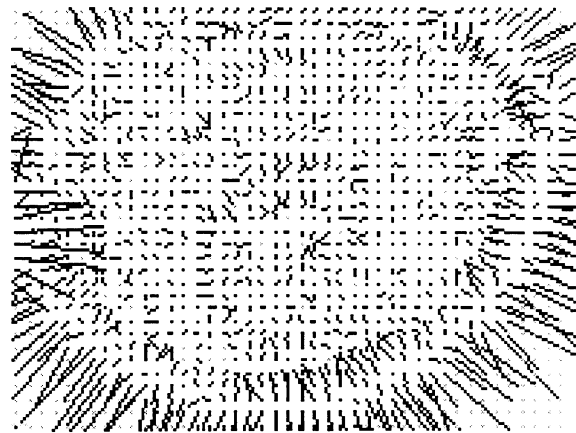In general, measurements at the 0.001 μm level are very

Figure 8 - Wavefront slope vector plot for fused silica rod homogeneity test. Note the strong ring structures on the interior of the rod. The strong edge effects are due to partial sampling of some focal spots, and, since the intensity at these points is low, have little effect on the results.

difficult, since air movement and temperature gradients degrade the results. However most optics have variations much greater than 0.01 μm, so 0.001 μm sensitivity is not required. If higher sensitivity is necessary, the sensor and optics under test can be shrouded to minimize the effects of air turbulence. It should be noted that when there is noise due to air turbulence, it straightforward to rapidly acquire successive images at the maximum frame rate (currently 11 Hz for the CLAS-2D Ver. 1.0), and average the results. This is difficult with interferometers since the data acquisition period is comparatively long, and air turbulence, vibrations and other perturbations can cause changes in the optical phase during the measurement.

Figure 10 shows another example measurement, and demonstrates the versatility of this optical metrology system. Here we measured the homogeneity of a 5 mm diameter, 6 mm long fused silica rod. Because the rod diameter was only 5 mm, it was placed in the small diameter part of the optical path, adjacent to the beamsplitter, in a double pass configuration. The rod was known to have poor homogeneity, and the test clearly shows a ring like structure throughout the
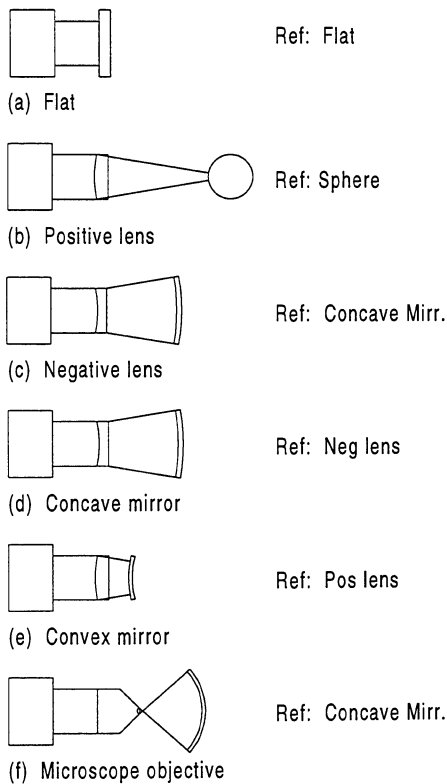

(a) Flat   Ref: Flat

(b) Positive lens   Ref: Sphere

(c) Negative lens   Ref: Concave Mirr.

(d) Concave mirror   Ref: Neg lens

(e) Convex mirror   Ref: Pos lens

(f) Microscope objective   Ref: Concave Mirr.

Figure 11 - Classical test configurations for various kinds of optics. Each of these configurations relies on a reference optic of known quality.

(a) Positive lens

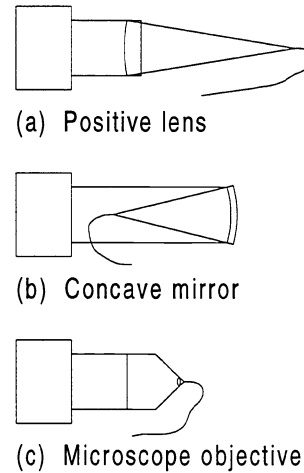(b) Concave mirror

(c) Microscope objective

Figure 12 - Test configurations for positive elements that use a single mode fiber as a reference. No other optics are needed in this configuration.

aperture. These structures are even more evident in the slope measurements and also show up in the intensity distribution. Similar tests have been conducted for YAG rods and other optical elements.

4. Measurement configurations

To be useful for optical testing, this instrument is required to be capable of testing a number of different types of optics. Flats, spheres, and aspheres, in both positive and negative configurations, need to be tested. Each of these requires a different test configuration. Classical test configurations are shown in Figure 11. In each of these configurations, the element is tested against a known reference optic. In many cases this can be a sphere. For positive lenses, ball bearings have been found to be nearly perfect spheres, and have excellent surface quality. For negative lenses, a high precision test mirror is needed. One problem is that the reference optics themselves must be tested somehow. Providing traceable standards for optics is difficult at best.

The optical metrology system we have described usually uses an its own internal light source in the "active mode". However, it has the advantage that it can test optical systems that include their own source light, or use an external source as a reference. This allows testing of certain optical elements in a single-pass configuration that we call the "passive mode". For example, a single mode fiber or pinhole can serve as the source for positive lenses. Light from the central region of such a source has a nearly perfect spherical wavefront, and is as close to an absolute reference as can be readily obtained. Figure 12 presents several test
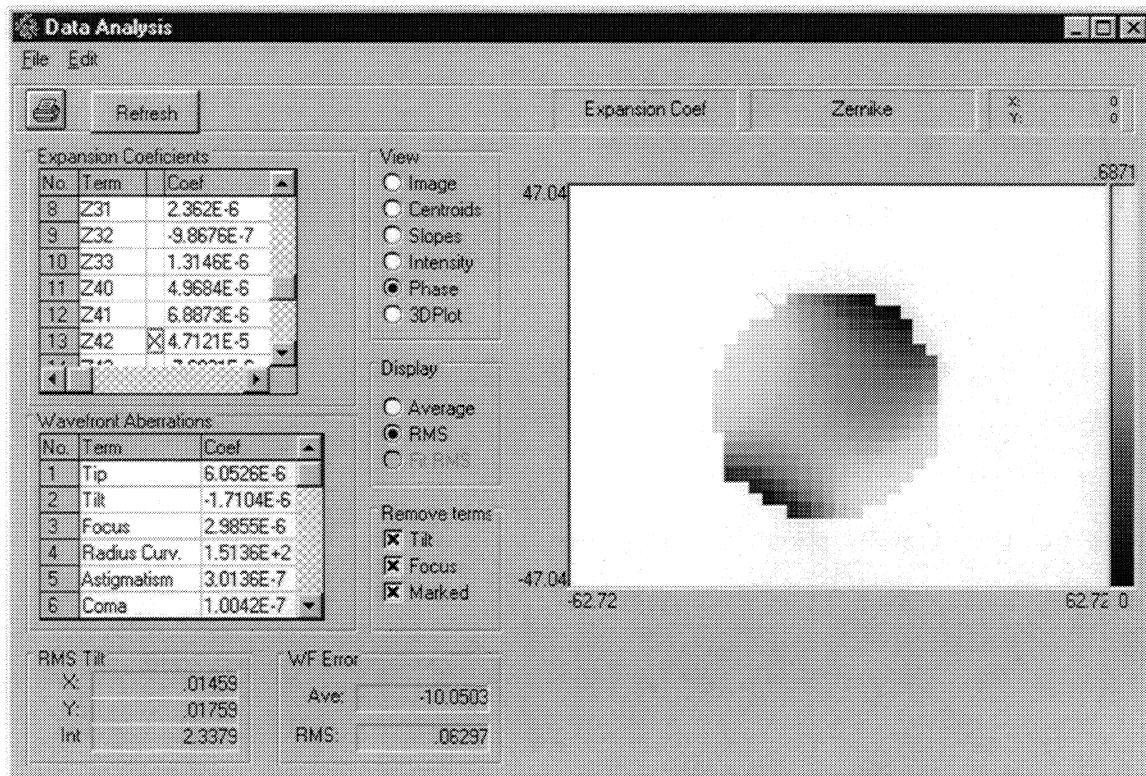
Figure 13 - Data analysis screen showing Zernike polynomials. The gray scale picture shows the wavefront after removal of the tilt, focus and spherical aberration terms.

configurations using this technique. These optical elements are designed to focus tightly, so they are properly characterized by testing them against a "point source." To make these tests using the instrument described here, the fiber input to the beam expander is removed and used as the external source. The test configuration is both simple and accurate because no reference optics are required.

5. Results

As an example of testing optics with this system, a test of a positive achromatic lens was conducted using broad band light. The test configuration is the same as shown in Figure 11 (b) with a 0.5 inch diameter ball bearing as the reference optic. This test was quite sensitive to the alignment of the lens and reference optics, so the ball bearing was placed on a three-axis stage to allow accurate alignment. The wavefront sensor was used in continuous acquisition mode to repeatedly reconstruct the wavefront while the ball bearing position was adjusted to minimize the total RMS wavefront error. The results of this test were shown previously as examples in Figure 2 and 4. While the phase maps are informative, it is somewhat easier to interpret a fit of the wavefront to Zernike polynomials. Figure 13 shows a

data analysis screen for calculating and displaying wavefront fits to Zernike polynomials. With tilt, focus, and spherical aberration terms removed, the residual wavefront error is 0.063 μm, compared to 0.615 μm with only tilt and focus removed, indicating that most of the residual aberration is spherical. The remaining terms show some 45 degree astigmatism. Fitting to Zernike or other polynomials provides convenient interpretation of the wavefront in well understood terms.

6. Conclusions

We have developed an instrument for optical metrology that is based on a Shack-Hartmann wavefront sensor. The sensor is integrated with a beam expander, light source, and other optics to produce a complete system that can be used for optics testing and characterization. The unit is versatile and robust, providing passive or active testing of optics up to 100 mm diameter.

Optics can be tested in many different configurations, including new configurations that take advantage of the passive nature of the wavefront sensor. An external source consisting of a single mode fiber or pinhole can be used for absolute calibration or testing.

Magnification is an important parameter for the design of an optical metrology system incorporating a wavefront sensor. Magnification allows testing of large diameter optics and greatly increases sensitivity, but it decreases dynamic range at the same time. If a large dynamic range is required, it can be readily obtained by using different lenslet arrays that have a smaller f/#.

7. References

[1] D. Malacara, *Optical Shop Testing*, 2nd ed.,(John Wiley and Sons, Inc., New York, 1992), pp. 265–295.

[2] K. Creath, "WYKO systems for optical metrology," SPIE **816**, 111 (1987b).

[3] K. Creath, "Phase-measurement interferometry techniques," in *Progress in Optics*, Vol. XXVI, E. Wolf, Ed., Elsevier Science Publishers, Amsterdam, 1988, pp. 349-393.

[4] D. R. Neal, W. J. Alford, J. K. Gruetzner, and M. E. Warren, "Amplitude and phase beam characterization using a two-dimensional wavefront sensor," SPIE Vol. 2870, 72–81 (1996).

[5] D. Kwo, G. Damas, and W. Zmek, "A Hartmann-Shack wavefront sensor using a binary optic lenslet array," SPIE Vol. 1544, 66–74 (1991).

[6] Strictly speaking, the wavefront sensor measures irradiance (W/m^2) and phase. In the past, intensity was used to denote power per unit area, but irradiance has now taken this definition. In this paper, intensity will still denote W/m^2. The photometric Intensity (W/Sr) can be derived from the irradiance and phase. See for example E. Hecht and A. Zajac, *Optics*, (Addison-Wesley, 1979, Menlo Park, CA), pp. 46; M. Born and E. Wolf, *Principles of Optics*, (Pergamon Press, New York, 1980), pp. 182.

[7] W.H. Southwell, "Wave-front estimation from wavefront slope measurements," JOSA **70** (8), pp.993-1006 (August, 1980).

[8] D. Malacara, *Optical Shop Testing*, 2nd ed.,(John Wiley and Sons, Inc., New York, 1992), pp. 464–472.

[9] CLAS-2D is a trademark of WaveFront Sciences, Inc.

[10] D. Neal, R. Pierson, E. Chen, K. Bishop, and L. McMackin, "One dimensional wavefront sensor development for tomographic flow measurements," SPIE Vol. 2546, 378–390 (1995).

[11] D. R. Neal, T. J. O'Hern. J. R. Torczynski, M. E. Warren, and R. Shul, "Wavefront sensors for optical diagnostics in fluid mechanics: application to heated flow, turbulence and droplet evaporation," SPIE Vol. 2005, 194–203 (1993).